

Implications of the AMS-02 positron fraction in cosmic rays

Qiang Yuan^a, Xiao-Jun Bi^{a1}, Guo-Ming Chen^a, Yi-Qing Guo^a, Su-Jie Lin^a,
Xinmin Zhang^b

^a*Key Laboratory of Particle Astrophysics, Institute of High Energy Physics, Chinese Academy of Science, Beijing 100049, P.R.China*

^b*Theoretical Physics Division, Institute of High Energy Physics, Chinese Academy of Sciences, Beijing 10049, P.R. China*

Abstract

The AMS-02 collaboration has just released its first result of the cosmic positron fraction $e^+/(e^- + e^+)$ with high precision up to ~ 350 GeV. The AMS-02 result shows the same trend with the previous PAMELA result, which requires extra electron/positron sources on top of the conventional cosmic ray background, either from astrophysical sources or from dark matter annihilation/decay. In this paper we try to figure out the nature of the extra sources by fitting to the AMS-02 $e^+/(e^- + e^+)$ data, as well as the electron and proton spectra by PAMELA and the $(e^- + e^+)$ spectrum by Fermi and HESS. We adopt the GALPROP package to calculate the propagation of the Galactic cosmic rays and the Markov Chain Monte Carlo sampler to do the fit. We find that under the conventional assumptions about the background and the extra source of the $e^- + e^+$, we cannot fit the AMS-02 and Fermi/HESS data well simultaneously. The AMS-02 data require less electrons/positrons from the extra sources than that required by Fermi/HESS. It may indicate that the model needs to be refined or the data between these experiments have systematic uncertainties. The pulsar scenario generally fits the data better than the DM scenario. Furthermore, the constraints from γ -rays also disfavor the DM scenario to explain the cosmic ray lepton data.

¹The corresponding author (email: bixj@ihep.ac.cn)

1. Introduction

The Alpha Magnetic Spectrometer (AMS-02) was launched in May 2011. After nearly two years operation and analysis, the AMS-02 collaboration has released its first physical result, i.e. the positron fraction $e^+/(e^- + e^+)$ in cosmic rays (CRs) [1]. The data show very high precision with the energy range from ~ 0.5 GeV to ~ 350 GeV. The fraction rises above ~ 8 GeV up to the energy end at ~ 350 GeV, which is consistent with the previous PAMELA result of the cosmic positron fraction [2, 3]. The result is NOT consistent with the conventional CR expectation [4]. A great number of works have dedicated to explaining the PAMELA result, either by astrophysical sources [5, 6, 7, 8, 9, 10] or by dark matter (DM) [11, 12, 13, 14, 15].

To determine the parameters of the CR background and the nature of the extra sources we have to consider all the relevant results. The available results at present include the pure electron spectrum measured by PAMELA [16] and the antiproton flux and ratio \bar{p}/p [17, 18] by PAMELA. Another important result from PAMELA is the precise measurement of the proton spectrum [19], which determines the secondary positron spectrum by collision with the interstellar medium (ISM) when propagating in the Galaxy. There are also precise measurements of the total electron and positron ($e^- + e^+$) spectrum, by the Fermi-LAT collaboration [20, 21] and ATIC collaboration [22]. The ground-based atmospheric Cerenkov telescopes HESS also gives measurement of the total e^\pm spectrum up to higher energies [23, 24].

Fitting to the PAMELA positron fraction data [2], PAMELA electron spectrum and Fermi/HESS total e^\pm spectrum shows that both the astrophysical source, such as pulsars, and the DM scenarios can give a good explanation to the data [4]. It is hard to discriminate the two scenarios with the CR spectra mentioned above. As the AMS-02 data show much higher precision and wider energy extension, especially it shows softer behavior than the PAMELA 2008 result, it is necessary to re-examine the previous conclusion with all of the newly available data. In this work we have done such a global fitting to all the relevant data, including AMS-02 $e^+/(e^- + e^+)$, Fermi and HESS ($e^- + e^+$) total spectrum and PAMELA proton and electron spectra.

We adopt the CosRayMC code, which embeds the CR propagation code in the Markov Chain Monte Carlo (MCMC) sampler and enables efficient survey of the high-dimensional parameter space [25, 4]. The CR propagation is treated by the GALPROP package [26]. The CR transportation process in the Galaxy is characterized by the secondary particles. Therefore the

secondary-to-primary ratio, such as B/C, (Sc+Ti+V)/Fe, and the unstable-to-stable ratio of secondary particles, such as $^{10}\text{Be}/^9\text{Be}$, $^{26}\text{Al}/^{27}\text{Al}$ are often used to determine the propagation parameters [27, 26, 28, 29]. In this work we fix the CR propagation parameters to the values which give the best fitting to the currently available B/C and $^{10}\text{Be}/^9\text{Be}$ data with the MCMC method. The fitting process will be reported separately in [30].

We then fit the parameters of the electrons and positrons to the relevant data, both from the CR background and the extra sources. We emphasize that the global fitting is important because when both components contribute to the observations neither one should be determined separately. In the work we have considered the continuously distributed pulsars² and DM annihilation/decay as two typical scenarios of the extra positron/electron sources. Note that this assumption may be over-simplified, because for energies up to hundreds of GeV the variance comes from discrete distribution of the sources can be very important. The discreteness will make the problem more complicated and uncertain. The current data may not be able to discriminate the continuous scenario from discrete scenario. However, the phenomenological consequences of both scenarios, i.e., the locally spectra of e^\pm should be similar in order to match the data. The injection parameters of primary electrons are free parameters to be fitted. The cosmic positrons include secondaries from CR interaction with the ISM and the primary ones from the extra sources. The secondary positron spectrum is determined by the spectrum of cosmic protons (including Helium and a few heavier nuclei) and the primary positron spectrum is determined by the nature of the extra sources. In principle the injection parameters of the protons can be fitted independently and then be employed to calculate the secondary positrons. However, since both the proton and electron spectra are measured by PAMELA at almost the same time, they are modulated by the solar activity with a similar magnitude. Therefore, in this work we have adopted two ways to fit the cosmic proton injection parameters: either by fitting the proton spectrum independently or by fitting the proton and electron spectra simultaneously.

This paper is organized as follows. We give a brief introduce of the propagation of Galactic CRs in Sec. 2. The experimental data and fitting method are described in Sec. 3. The results are presented in Sec. 4. In Sec.

²In the following part of this paper, “pulsar” actually means the pulsar-like astrophysical sources which can produce e^\pm pairs.

5 we give discussion about the fitting results, and finally a brief summary is given in Sec. 6.

2. Cosmic ray propagation

The propagation of charged CRs in the Galaxy is described by the diffusive equation [31]

$$\begin{aligned} \frac{\partial \psi}{\partial t} = & Q(\mathbf{x}, p) + \nabla \cdot (D_{xx} \nabla \psi - \mathbf{V}_c \psi) + \frac{\partial}{\partial p} p^2 D_{pp} \frac{\partial}{\partial p} \frac{1}{p^2} \psi \\ & - \frac{\partial}{\partial p} \left[\dot{p} \psi - \frac{p}{3} (\nabla \cdot \mathbf{V}_c \psi) \right] - \frac{\psi}{\tau_f} - \frac{\psi}{\tau_r}, \end{aligned} \quad (1)$$

where ψ is the density of CR particles per unit momentum interval, $Q(\mathbf{x}, p)$ is the source term, D_{xx} is the spatial diffusion coefficient, \mathbf{V}_c is the convection velocity, D_{pp} is the diffusion coefficient in momentum space used to describe the reacceleration process, $\dot{p} \equiv dp/dt$ is the momentum loss rate, τ_f and τ_r are time scales for fragmentation and radioactive decay respectively. D_{xx} is usually assumed to be only rigidity dependent and has a power-law form $D_{xx} = D_0 \beta (R/R_0)^\delta$, with δ reflecting the property of the interstellar medium (ISM) turbulence. The reacceleration is described by the diffusion in momentum space. The momentum diffusion coefficient D_{pp} relates with the spatial diffusion coefficient D_{xx} as [32]

$$D_{pp} D_{xx} = \frac{4p^2 v_A^2}{3\delta(4 - \delta^2)(4 - \delta)w}, \quad (2)$$

where v_A is the Alfvén speed, w is the ratio of magnetohydrodynamic wave energy density to the magnetic field energy density, which characterizes the level of turbulence. In the usual way we take w to be 1 and use the Alfvén speed v_A to describe the reacceleration [32]. The CRs propagate in an extended halo with characteristic height z_h , beyond which free escape of CRs is assumed. Thus the major propagation parameters include D_0 , δ , v_A , V_c and z_h .

There are publicly available numerical codes to compute the CRs propagation in the Galaxy, such as GALPROP³ [26] and DRAGON⁴ [33]. We

³<http://galprop.stanford.edu/>

⁴<http://www.desy.de/~maccione/DRAGON/>

have embedded the GALPROP package with the MCMC sampler and fitted to the data to constrain the propagation parameters [30].

Table 1: Propagation parameters taken in the work

$D_0(10^{28} \text{ cm}^2\text{s}^{-1})^1$	5.94
δ	0.377
$z_h(\text{kpc})$	4.04
$v_A(\text{km s}^{-1})$	36.4

¹At $R_0 = 4 \text{ GV}$.

Recently several groups employed the MCMC technique to fit the CR propagation parameters [34, 35, 36]. Using the currently available data of B/C and ¹⁰Be/⁹Be, we did an independent MCMC fit to the propagation parameters [30]. We find the reacceleration model gives quite good description to the present data, while the convection model gives worse fitting. Therefore we adopt the reacceleration (i.e., $V_c = 0$) scenario as the starting point of the present study. The values of the propagation parameters we adopted in the work are listed in Table 1, as given in [30]. We have tested that varying the propagation parameters within extreme ranges allowed by the B/C data [37], the qualitative results of this work do not change.

3. Fitting description

3.1. Model

The basic framework of the CR model is as follows. The primary sources of CRs, such as the supernova remnants (SNRs), accelerate CR nuclei and electrons and inject them into the Galaxy. These particles then propagate in the Galaxy, experiencing diffusion, reacceleration, interactions and radiation during the propagation process. The interactions with ISM produce secondary particles including the secondary nuclei (such as Li, Be, B, and Sc, Ti, V), positrons, antiprotons and diffuse γ -rays. Such a scenario gives consistent description of most of the CR data as well as the all-sky diffuse γ -ray emission [31]. To distinguish from the extra sources of the e^\pm as will be described below, we call this component as the background. The model to fit the AMS-02 data includes this CR background (primary nuclei and electrons, and the secondary positrons) and the extra positron/electron sources.

The injection spectra of the primary protons (heavier nuclei are less relevant) and electrons are assumed to be broken power-law functions with respect to the momentum p

$$q(p) \propto \left(\frac{p}{p_{\text{br}}^{p,e}} \right)^{-\nu_1/\nu_2}, \quad (3)$$

where ν_1 and ν_2 are the spectral indices below and above the break momentum p_{br} . In the following we use ν_1 and ν_2 to represent the proton spectrum and use γ_1 and γ_2 to represent the primary electron spectrum. The propagated fluxes of protons and electrons are then normalized to factors A_p and A_e to get the absolute fluxes.

The spatial distribution of the primary CR particles is adopted to be the supernova remnants (SNR) like distribution

$$f(R, z) \propto \left(\frac{R}{R_\odot} \right)^a \exp \left[-\frac{b(R - R_\odot)}{R_\odot} \right] \exp \left(-\frac{|z|}{z_s} \right), \quad (4)$$

where $R_\odot = 8.5$ kpc is the distance of solar system from the Galactic center, $z_s \approx 0.2$ kpc is the characteristic height of the Galactic disk, a and b are the shape parameters which can be fitted according to the survey data of SNRs or other kinds of assumed CR sources. We employ $a = 1.25$ and $b = 3.56$ following [36].

For the secondary electrons/positrons we adopt the same GALPROP model to calculate their propagation. The production spectra of the secondary electrons/positrons are calculated using the parameterization given in [38] based on the propagated proton spectrum. A free factor c_{e^+} to normalize the secondary positron/electron flux is included in the fitting, which represents the possible uncertainties from the hadronic interactions, propagation models, the ISM density distributions, and the nuclear enhancement factor from heavy elements. A caveat is that the nuclear collision may not be simply scaled from the pp collision, i.e., the nuclear enhancement factor is energy dependent [39]. Since the energy dependence is weak, we keep the constant factor as an approximation here.

About the extra electron/positron sources, we study two popular kinds of sources: the astrophysical sources such as pulsars and the DM annihilation scenario. The injection spectrum of the astrophysical sources is parameterized as a power-law function with an exponential cutoff

$$q(p) = A_{\text{psr}} p^{-\alpha} \exp(-p/p_c), \quad (5)$$

where A_{psr} is the normalization factor, α is the spectral index and p_c is the cutoff momentum. The source population is taken to be a continuous form with distribution function (4), but with different parameters $a = 2.35$ and $b = 5.56$, given in [40]. The effect of nearby isolate sources (e.g., [6, 5, 7], see also the discussion in Sec. V) is not covered in the present study. Note there were proposals that the hadronic interactions around the CR sources and the subsequent acceleration of the secondary e^\pm could be responsible for the e^\pm excesses [10, 41]. Such a scenario is not in conflict with the pulsar-like scenario assumed here (with slight difference of the spatial distribution which has little effect on the charged CR propagation). But we should keep in mind the simultaneously produced antiprotons and secondary nuclei may constrain this model [42, 43, 44].

For the DM annihilation scenario, the density profile of the Milky Way halo is adopted to be the Navarro-Frenk-White (NFW) distribution [45]

$$\rho(r) = \frac{\rho_s}{(r/r_s)(1 + r/r_s)^2}, \quad (6)$$

with $r_s = 20$ kpc and $\rho_s = 0.26$ GeV cm $^{-3}$. Such a value of ρ_s will correspond to a local density of 0.3 GeV cm $^{-3}$. For higher values of the local density as revealed by several recent studies [46, 47, 48], the annihilation cross section will be different by a constant factor. Since the measurement of CR antiprotons by PAMELA [17, 18] constrain the hadronic annihilation channels strongly [13, 14, 49, 50], we will focus on the leptonic annihilation channels here. The positron spectrum from the DM annihilation products is calculated using the PYTHIA simulation package [51].

The CRs at low energy (typically with rigidity below ~ 30 GV) are affected by the solar environment when entering the solar system, known as solar modulation effect. The force field approximation is often employed to describe the solar modulation effect [52], which has only one single parameter — the modulation potential ϕ . However, the low energy data about the positron fraction measured by PAMELA and AMS-02 may imply that the simple force field approximation is not enough to explain the data, and the charge-sign dependent modulation effect is necessary [53, 54, 55]. Therefore, in order to avoid possible inconsistency of the low energy behavior we do not include the AMS-02 data below 5 GeV in our fit. The solar modulation effect for the positron fraction above 5 GeV is negligible [55, 56].

In summary the full parameter space investigated in this work is

$$\mathcal{P} = \begin{cases} \{A_p, \nu_1, \nu_2, p_{\text{br}}^p\}, & \text{bkg protons,} \\ \{A_e, \gamma_1, \gamma_2, p_{\text{br}}^e\}, & \text{bkg electrons,} \\ \{A_{\text{psr}}, \alpha, p_c\} \text{ or } \{m_\chi, \langle\sigma v\rangle, \text{ch}\}, & \text{exotic sources,} \\ \{c_{e^+}, \phi\}, & \text{others,} \end{cases} \quad (7)$$

where ‘‘ch’’ represents the channel of DM annihilation, which is set to be one of $\{\mu^+\mu^-, \tau^+\tau^-, W^+W^-, b\bar{b}\}$ and does not enter in the fitting. Such a model works well for the PAMELA and Fermi data [4].

3.2. Data

Table 2: Definition of fitting

I-a	AMS e^+/e^\pm + PAMELA e^- + Fermi/HESS e^\pm
II-a	AMS e^+/e^\pm + PAMELA e^-
I-b	AMS e^+/e^\pm + PAMELA e^- + Fermi/HESS e^\pm + PAMELA p
II-b	AMS e^+/e^\pm + PAMELA e^- + PAMELA p

In this study the data to be fitted include the latest positron fraction by AMS-02[1], the electron spectrum by PAMELA [16], the total electron and positron spectra by Fermi [20, 21] and HESS [23, 24], and the proton spectrum by PAMELA [19]. We choose two ways to deal with the proton spectrum as described in Sec. I: a) to fit it separately, and b) to include it in the global fitting.

Note that the CR spectral hardening at ~ 200 GV reported by ATIC [57], CREAM [58] and PAMELA [19] implies that single power-law can not fully describe the high energy spectra of the CR nuclei above ~ 10 GV⁵. Therefore we only take the PAMELA proton data below 150 GeV in the fit. To better fit the high energy part (and the CREAM data), we need a further break or a curved injection spectrum of the protons [60].

Since the Fermi and HESS data may have larger systematic uncertainties we also investigate the case without the Fermi/HESS data. The definition of the fittings are compiled in Table 2.

⁵Note, however, the preliminary data about the proton and Helium spectra show no hardening below \sim TeV [59]. Combining with the CREAM data, it may still show a hardening of these spectra at higher energies.

4. Results

4.1. Fixing the proton spectrum

We first fit the proton spectrum independently with the PAMELA (and CREAM) data. Here we add the high energy CREAM data [58] in the fitting to give a description of the proton behavior in a wider energy range. The best fitting injection parameters of protons are: $\nu_1 = 1.79$, $\nu_2 = 2.36$, $p_{\text{br}}^p = 11.7$ GeV and the solar modulation potential $\phi = 470$ MV. The propagated proton spectrum for the best fitting parameters is shown in Fig. 1.

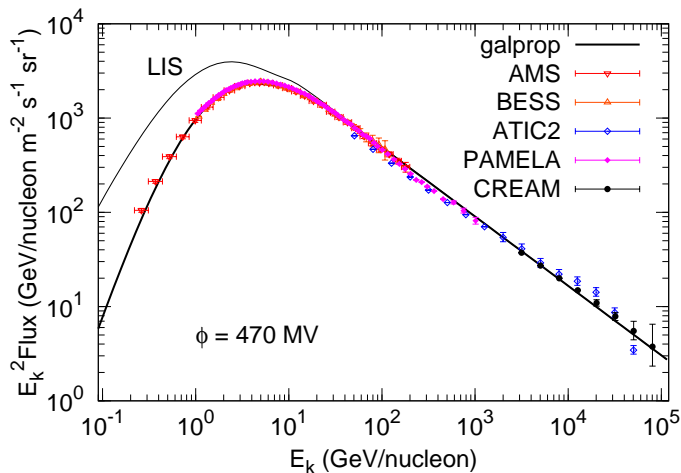


Figure 1: Proton spectrum derived through fitting PAMELA data. References of the proton data: AMS [61], BESS [62], ATIC2 [57], PAMELA [19] and CREAM [58].

We then run the fits I-a, II-a to derive the parameters of CR electrons/positrons with the best fitting proton spectrum. The resulting positron fraction and electron spectrum for the best fitting parameters of each fit, for both the pulsar and DM scenarios, are shown in Figs. 2 - 4. For each figure, the panels from left to right correspond to the fits I-a and II-a respectively. The best fitting parameters, mean values and their 1σ uncertainties are compiled in Tables 3 - 5, and the best fitting χ^2 over the number of degree of freedom (dof) are given in Table 6.

From Fig. 2 we can see that adding a pulsar component can roughly reproduce the AMS-02 positron fraction data and the Fermi/HESS total electron spectra. However, the fitting seems not good enough. The model prediction overproduces the positron fraction compared with AMS-02 data but

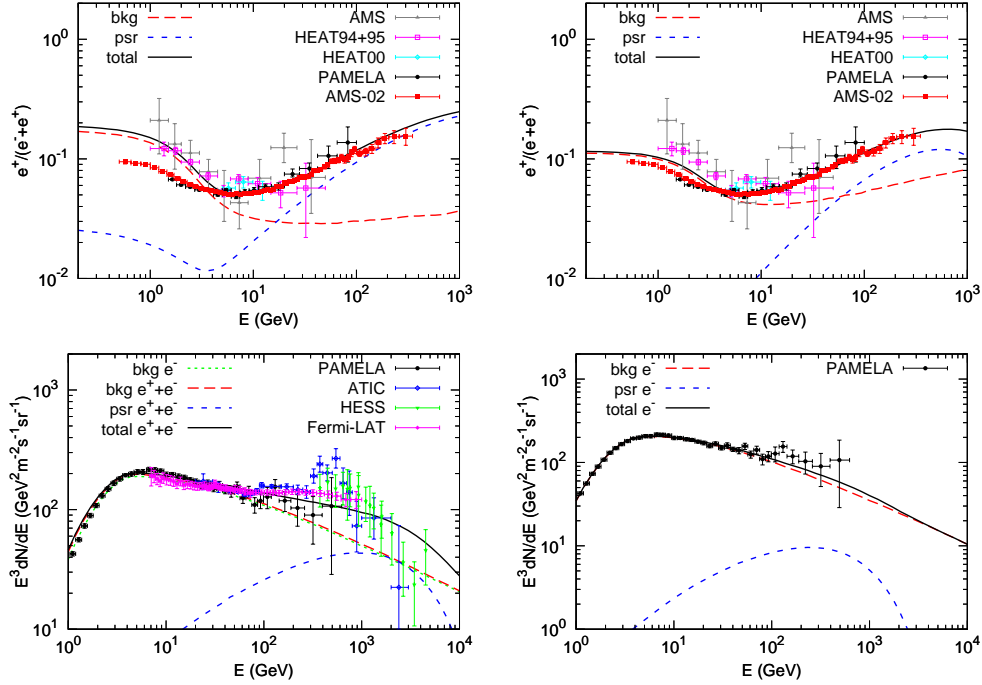


Figure 2: The positron fraction (upper) and electron spectra (lower) for the background together with a pulsar component of the exotic e^\pm . The panels from left to right are for fits I-a and II-a respectively. References of the data: positron fraction — AMS [63], HEAT94+95 [64], HEAT00 [65], PAMELA [2], AMS-02[1] ; electron — PAMELA [16], ATIC [22], HESS [23, 24], Fermi-LAT [21].

underproduces total e^+e^- spectra compared with Fermi/HESS data. This is clearly seen from the fits II-a, in which the constraints of Fermi/HESS data are removed. We see that the fit II-a gives good fit to the AMS-02 data, but deviate from the Fermi data more obviously. It may indicate that the model described in Sec. 3.1 needs to be refined, or there is a *tension* between the AMS-02 positron fraction and the Fermi/HESS electron spectra⁶. Quanti-

⁶The recently reported e^\pm spectra measured by AMS-02 do show the discrepancy with the Fermi data [59], which is however, most apparent at low energies. We test the fit I-a with only the Fermi data above 70 GeV, the χ^2/dof is about 147/114, which means the tension still exists and the basic conclusion does not change even we drop the low energy Fermi data. Better determination of the high energy behavior of the e^\pm spectra by AMS-02 is necessary to finally solve this problem.

Table 3: Fitting results of pulsar model with proton spectrum fixed

	I-a		II-a	
	best	mean	best	mean
$\log(A_e^1)$	-8.978	-8.974 ± 0.005	-8.925	-8.921 ± 0.011
γ_1	1.504	1.512 ± 0.010	1.708	1.704 ± 0.084
γ_2	2.645	2.652 ± 0.010	2.794	2.796 ± 0.028
$\log(p_{\text{br}}^e/\text{MeV})$	3.599	3.587 ± 0.022	3.597	3.600 ± 0.046
$\log(A_{\text{psr}}^2)$	-24.867	-24.918 ± 0.146	-25.257	-25.226 ± 0.562
α	1.912	1.903 ± 0.029	1.856	1.863 ± 0.116
$\log(p_c/\text{MeV})$	6.640	6.632 ± 0.111	5.927	6.097 ± 0.412
c_{e^+}	1.272	1.327 ± 0.075	2.206	2.222 ± 0.242
ϕ/MV	500	527 ± 30	818	830 ± 72

¹Normalization at 25 GeV in unit of $\text{cm}^{-2}\text{s}^{-1}\text{sr}^{-1}\text{MeV}^{-1}$.

²Normalization at 1 MeV in unit of $\text{cm}^{-3}\text{s}^{-1}\text{MeV}^{-1}$.

tatively, the best fitting χ^2 is about 279 for fit I-a. For 151 dof such a χ^2 means $\sim 6.1\sigma$ deviation from what expected. Similar conclusion has also been derived in [13, 66, 67].

Compared with the fitting results with PAMELA positron fraction data [4], the spectrum of the pulsar component becomes much softer (with power-law index ~ 1.9), which may be more reasonable according to the pulsar modeling [7]. The contribution of e^\pm from the pulsars is also smaller than previous estimated according to the PAMELA data. Our fit shows that up to TeV the positron fraction is only $\sim 20\%$, while it is more than 30% or even reaching 40% according to the fitting to the PAMELA data.

Figs. 3 and 4 give the results for the DM annihilation scenario. The fitting results are even worse than the pulsar scenario. For DM annihilation into $\mu^+\mu^-$, the reduced χ^2 for fit I-a is as high as 3.3. The reason of the poor fit is that the positron spectrum from DM annihilation to a pair of $\mu^+\mu^-$ is too hard. This can be seen from the top-left panel of Fig. 3. The DM component will over-produce high energy positrons (> 100 GeV) but under-produce positrons at tens of GeV. For fits I-a, heavy DM with mass $\sim 2 - 3$ TeV is required due to the constraints of Fermi/HESS data. If we throw away the Fermi/HESS e^\pm data (fit II-a), we find the AMS-02 data tend to favor lighter DM particles. In this case the 10 - 50 GeV AMS-02 data can be better reproduced, however, the data above 100 GeV are still difficult to

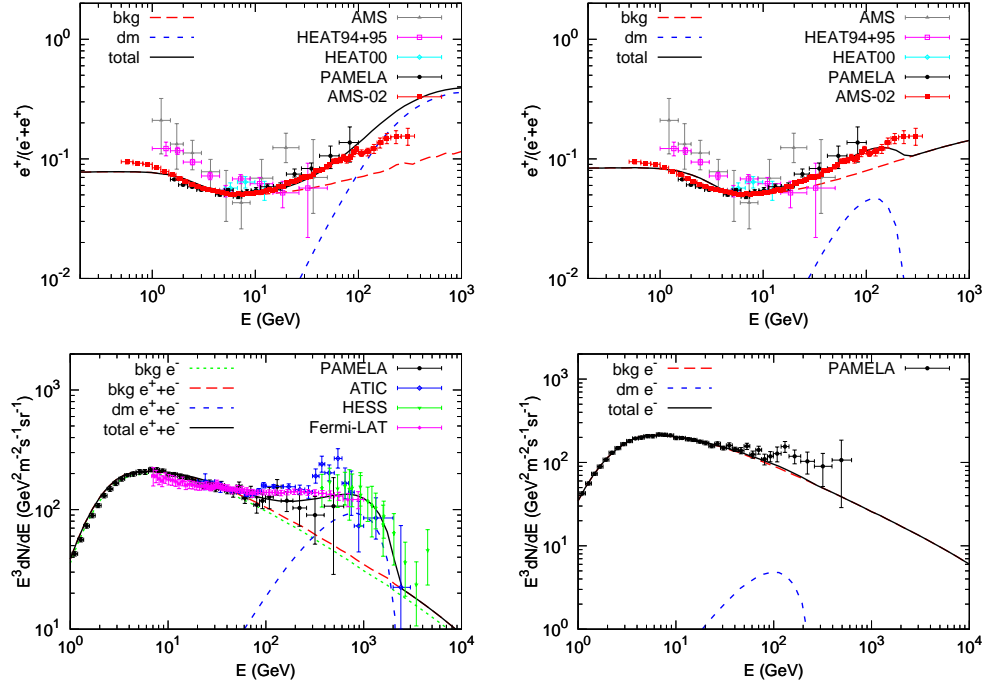


Figure 3: Same as Fig. 2 but the exotic e^\pm are assumed to be from DM annihilation. The annihilation channel is $\mu^+\mu^-$.

Table 4: Fitting results of DM annihilation to $\mu^+\mu^-$ with proton spectrum fixed

	I-a		II-a	
	best	mean	best	mean
$\log(A_e^1)$	-8.916	-8.916 ± 0.003	-8.915	-8.918 ± 0.006
γ_1	1.894	1.870 ± 0.036	1.896	1.868 ± 0.036
γ_2	2.839	2.839 ± 0.006	2.904	2.906 ± 0.014
$\log(p_{\text{br}}^e/\text{MeV})$	3.608	3.592 ± 0.035	3.692	3.674 ± 0.037
$\log(m_\chi/\text{GeV})$	3.371	3.368 ± 0.039	2.415	2.423 ± 0.039
$\log(\langle\sigma v\rangle/\text{cm}^3\text{s}^{-1})$	-22.307	-22.313 ± 0.067	-24.169	-24.166 ± 0.069
c_{e^+}	2.881	2.881 ± 0.030	3.052	3.038 ± 0.047
ϕ/MV	999	996 ± 4	999	991 ± 8

¹Normalization at 25 GeV in unit of $\text{cm}^{-2}\text{s}^{-1}\text{sr}^{-1}\text{MeV}^{-1}$.

be explained. Due to the lack of constraints from high energy data, this fit may under-estimate the contribution to the e^\pm excess from DM annihilation.

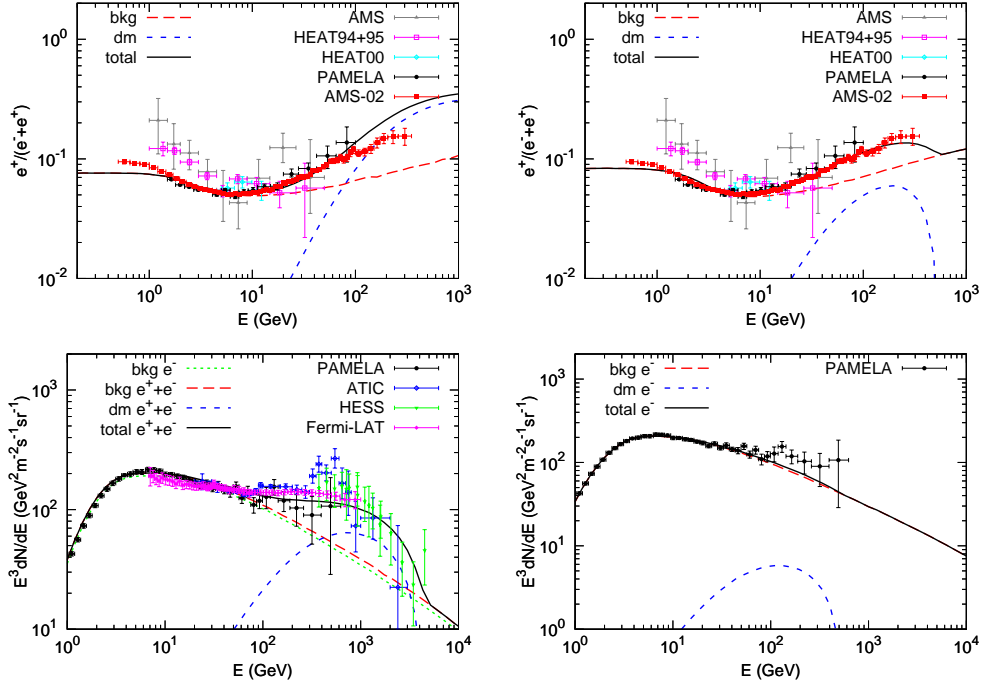


Figure 4: Same as Fig. 2 but the exotic e^\pm are assumed to be from DM annihilation. The annihilation channel is $\tau^+\tau^-$.

Table 5: Fitting results of DM annihilation to $\tau^+\tau^-$ with proton spectrum fixed

	I-a		II-a	
	best	mean	best	mean
$\log(A_e^1)$	-8.915	-8.916 ± 0.003	-8.907	-8.909 ± 0.006
γ_1	1.879	1.878 ± 0.037	1.869	1.817 ± 0.070
γ_2	2.813	2.813 ± 0.007	2.863	2.856 ± 0.015
$\log(p_{br}^e/\text{MeV})$	3.570	3.571 ± 0.037	3.637	3.608 ± 0.058
$\log(m_\chi/\text{GeV})$	3.667	3.665 ± 0.045	2.765	2.747 ± 0.046
$\log(\langle\sigma v\rangle/\text{cm}^3\text{s}^{-1})$	-21.699	-21.703 ± 0.073	-23.261	-23.269 ± 0.064
c_{e+}	2.773	2.769 ± 0.035	2.900	2.844 ± 0.068
ϕ/MV	999	994 ± 5	998	974 ± 20

¹Normalization at 25 GeV in unit of $\text{cm}^{-2}\text{s}^{-1}\text{sr}^{-1}\text{MeV}^{-1}$.

The situation for $\tau^+\tau^-$ final state is better. Similar with the $\mu^+\mu^-$ channel, the positron spectrum from tauon decay is still too hard. Relaxing the

constraints from Fermi/HESS data we find a lighter DM mass, $\sim 550 - 750$ GeV is favored. In this case the AMS-02 data can be fitted relatively well. It is interesting to note that even only the AMS-02 data and PAMELA electron data are considered (fit II-a), the mass of DM particles can be constrained in a small region. Such a strong constraint comes from the very high precise AMS-02 data at lower energy (a few tens GeV). However, since Fermi and HESS do observe plenty of electrons/positrons up to TeV energies, and no hint of significant drop of the total e^+e^- spectra is shown below TeV. Therefore, we should not take these values too seriously.

Table 6: Summary of fitting χ^2/dof . Note that the AMS-02 data above 5 GeV and PAMELA proton data below 150 GeV are used to calculate the χ^2 .

	pulsar	DM ($\mu^+\mu^-$)	DM ($\tau^+\tau^-$)
I-a	278.7/151	506.7/152	496.5/152
II-a	51.5/80	83.1/81	56.7/81
I-b	288.0/205	615.3/206	584.6/206
II-b	83.0/134	238.7/135	164.3/135

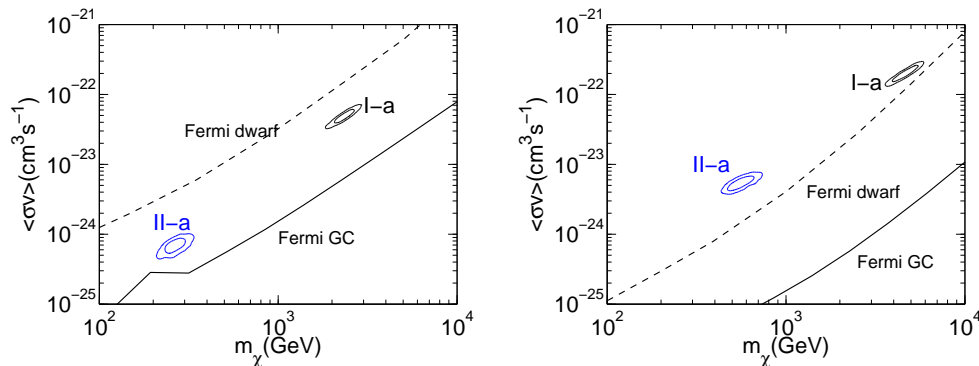


Figure 5: 1σ and 2σ confidence regions on the DM mass and cross section plane, for the fits I-a and II-a respectively. The left panel is for $\mu^+\mu^-$ channel, and the right panel is for $\tau^+\tau^-$ channel. The solid lines show the 95% upper limit of Fermi γ -ray observations of the Galactic center (with normalization of the local density corrected) [68] and dwarf galaxies [69].

Fig. 5 gives the 1σ and 2σ contour for the DM mass and annihilation cross section. But we should keep in mind that such results should not be considered statistically meaningful as the fits are quite bad. The solid lines

shown in Fig. 5 are the exclusion limits derived by the Fermi γ -ray observations of the Galactic center [68] and dwarf galaxies [69]. We can see that γ -rays tend to give strong constraints on the DM scenario, especially for the $\tau^+\tau^-$ final state. Note, however, the Galactic center results may suffer from uncertainties from the density profile. When calculating the γ -ray constraints the inverse Compton scattering component from the muon/tauon decaying electrons/positrons is not included, therefore these constraints should be somehow conservative.

It should be pointed out that fits II without Fermi/HESS data may underestimate the contribution to the e^\pm fluxes from the extra sources. The preliminary data of the electron spectrum by AMS-02 extend to ~ 500 GeV following the median values of PAMELA data without any features [59] also favors the existence of e^\pm excesses up to sub-TeV. Therefore we may be cautious to use the fits II to interpret the data because the lack of constraints from high energies will lead to improper understanding of the physics. The results of fits II may help understand the behaviors derived in fits I.

We further note that for the DM scenario, the parameter ϕ is very large. The solar modulation potential is assumed to vary between 300 and 1000 MV in these fits. From Tables 3 - 5 we see that almost in all cases the modulation potential tends to the upper end. This might be inconsistent with the fact that PAMELA and AMS-02 work approaching the solar minimum.

4.2. Relaxing the proton spectrum

Since the proton spectrum will affect the secondary positron production, and also the determination of the solar modulation parameter, we take the proton spectrum into account and redo the fits (labeled as I-b and II-b). The fitting results with the best fitting parameters are presented in Figs. 6-8. The mean values and the 1σ uncertainties of the model parameters are listed in Tables 7 - 9, and the best fitting χ^2 over dof are also presented in Table 6. Qualitatively we find that the results are similar with that in the previous subsection.

For the pulsar scenario, the minimum χ^2 for fit I-b is about 288, which corresponds to a $\sim 3.9\sigma$ deviation from what expected for 205 dof. Compared with the fits of fixed proton spectrum, the injection spectrum of positrons from pulsars is a little bit softer here. This is because the proton spectrum here is also softer than that in the previous subsection. Therefore a softer pulsar-induced positron spectrum is required to give more tens of GeV positrons and to compensate the effect of a softer proton spectrum.

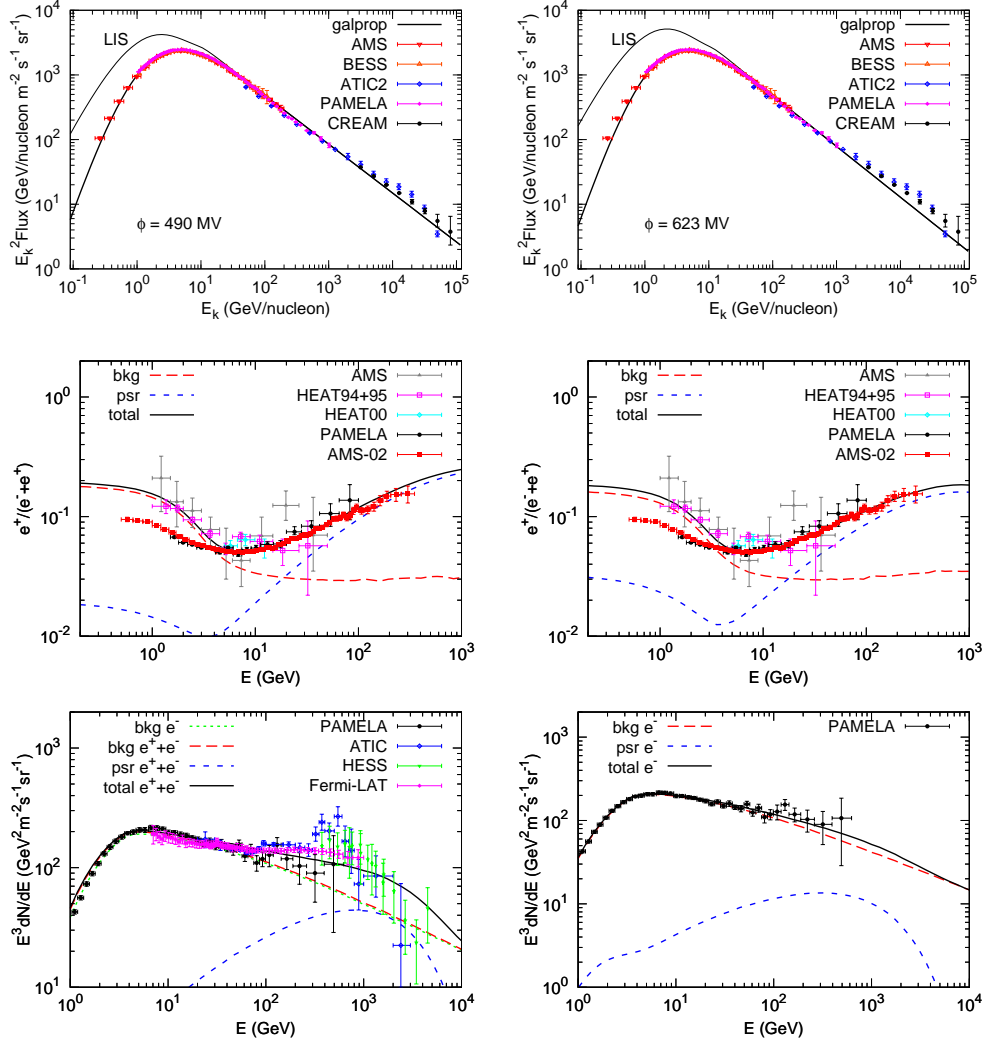


Figure 6: From top to bottom: the proton, positron fraction and electron spectra for the background together with a pulsar component of the exotic e^\pm . The left and right panels are for fits I-b and II-b respectively.

The DM scenario fits worse than the pulsar scenario. As we have discussed, the reason is that the DM-induced positron spectrum is too hard. The 1σ and 2σ confidence level contours on the $m_\chi - \langle\sigma v\rangle$ plane for the fits are shown in Fig. 9. The parameter regions differ only slightly from that derived in the previous subsection (Fig. 5). The strong constraints on the DM model from γ -rays are not changed.

Table 7: Fitting results of pulsar model with proton spectrum relaxed

	I-b		II-b	
	best	mean	best	mean
$\log(A_p^1)$	-8.323	-8.327 ± 0.005	-8.328	-8.330 ± 0.006
ν_1	1.789	1.797 ± 0.019	1.882	1.885 ± 0.023
ν_2	2.378	2.388 ± 0.011	2.410	2.415 ± 0.019
$\log(p_{\text{br}}^p/\text{MeV})$	4.040	4.064 ± 0.029	4.099	4.121 ± 0.031
$\log(A_e^2)$	-8.977	-8.979 ± 0.004	-8.941	-8.948 ± 0.008
γ_1	1.504	1.505 ± 0.004	1.535	1.554 ± 0.040
γ_2	2.647	2.645 ± 0.011	2.720	2.722 ± 0.018
$\log(p_{\text{br}}^e/\text{MeV})$	3.615	3.614 ± 0.015	3.614	3.631 ± 0.016
$\log(A_{\text{psr}}^3)$	-25.104	-25.012 ± 0.132	-24.494	-24.411 ± 0.335
α	1.864	1.881 ± 0.026	1.985	2.006 ± 0.068
$\log(p_c/\text{MeV})$	6.512	6.562 ± 0.093	6.205	6.442 ± 0.285
c_{e^+}	1.306	1.276 ± 0.062	1.503	1.468 ± 0.127
ϕ/MV	490	489 ± 21	623	614 ± 37

¹Normalization at 100 GeV in unit of $\text{cm}^{-2}\text{s}^{-1}\text{sr}^{-1}\text{MeV}^{-1}$.

²Normalization at 25 GeV in unit of $\text{cm}^{-2}\text{s}^{-1}\text{sr}^{-1}\text{MeV}^{-1}$.

³Normalization at 1 MeV in unit of $\text{cm}^{-3}\text{s}^{-1}\text{MeV}^{-1}$.

From Figs. 7 and 8 we note that the proton spectrum can not be well fitted for the DM scenario. This is also due to the hard positron spectrum from DM annihilation into muons and taus. A harder proton spectrum will produce more positrons above ~ 10 GeV, which will compensate the lack of positrons from the hard spectrum of the DM component. If we reduce the constraints from Fermi/HESS data (fits II-b), we see that the proton spectrum fits the data better.

We also note from Figs. 7 and 8 that when not including Fermi/HESS data the DM scenario does not give a good description to the high energy end of the AMS-02 data, which is different from the pulsar case shown in Fig. 6. This is because the positron spectrum is determined once the mass of DM and its annihilation final states are given. To have a minimum χ^2 the mass of DM (i.e. the shape of the positron spectrum) is usually determined by the data at tens of GeV where the errors are very small, instead of the behavior of the high energy end data.

The solar modulation potential ϕ and c_{e^+} at the DM case are larger than

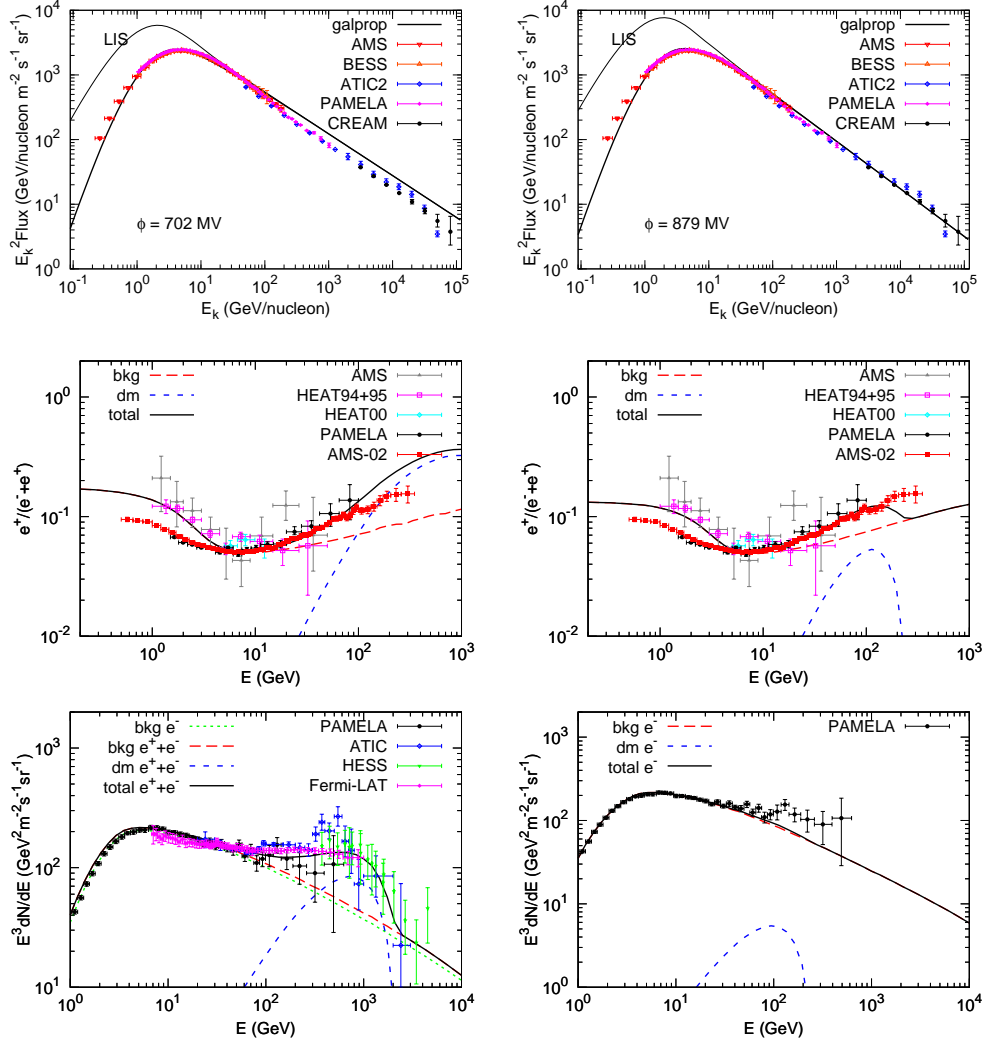


Figure 7: Same as Fig. 6 but the exotic e^\pm are assumed to be from DM annihilation. The annihilation channel is $\mu^+\mu^-$.

that in the pulsar case. The reason is that the DM spectrum is always harder than the pulsar case. To fit the AMS-02 data at tens of GeV, which are very precise, larger ϕ and c_{e^+} can give relatively higher flux of positrons in this energy range.

Table 8: Fitting results of DM annihilation into $\mu^+\mu^-$ with proton spectrum relaxed

	I-b		II-b	
	best	mean	best	mean
$\log(A_p^1)$	-8.275	-8.276 ± 0.004	-8.299	-8.298 ± 0.004
ν_1	1.936	1.947 ± 0.031	2.037	2.026 ± 0.022
ν_2	2.271	2.281 ± 0.009	2.364	2.365 ± 0.010
$\log(p_{\text{br}}^p/\text{MeV})$	3.919	3.929 ± 0.045	4.102	4.101 ± 0.035
$\log(A_e^2)$	-8.953	-8.950 ± 0.006	-8.938	-8.944 ± 0.008
γ_1	1.555	1.588 ± 0.054	1.789	1.754 ± 0.046
γ_2	2.768	2.773 ± 0.011	2.890	2.895 ± 0.016
$\log(p_{\text{br}}^e/\text{MeV})$	3.578	3.573 ± 0.027	3.679	3.670 ± 0.026
$\log(m_\chi/\text{GeV})$	3.330	3.338 ± 0.045	2.390	2.417 ± 0.038
$\log(\langle\sigma v\rangle/\text{cm}^3\text{s}^{-1})$	-22.397	-22.381 ± 0.076	-24.142	-24.117 ± 0.060
c_{e^+}	1.996	2.037 ± 0.064	2.541	2.527 ± 0.070
ϕ/MV	702	729 ± 39	879	866 ± 36

¹Normalization at 100 GeV in unit of $\text{cm}^{-2}\text{s}^{-1}\text{sr}^{-1}\text{MeV}^{-1}$.

²Normalization at 25 GeV in unit of $\text{cm}^{-2}\text{s}^{-1}\text{sr}^{-1}\text{MeV}^{-1}$.

4.3. Further tests

To better understand how soft a positron spectrum from the extra sources is needed, we show in Fig. 10 the 2σ range of source spectra from pulsars at the solar location with shaded regions. The 2σ range is defined with $\Delta\chi^2 = \chi^2 - \chi_{\text{min}}^2 = 22.7$ for 13 fitting parameters. For comparison the DM induced positron spectra for $\mu^+\mu^-$, $\tau^+\tau^-$, W^+W^- and $b\bar{b}$ channels are also shown. The mass of DM particle is taken to be $m_\chi = 1$ TeV and a free flux normalization is adopted. It is shown that the positron spectra from DM annihilation in the $\mu^+\mu^-$ and $\tau^+\tau^-$ channels are much harder than the pulsar component. For the W^+W^- and $b\bar{b}$ channels the spectrum is softer and we would expect a better fit to the data.

As a test we run the fit II-a with DM annihilation to W^+W^- and $b\bar{b}$ final states. We find the χ^2 values become slightly smaller (~ 52.7 for both W^+W^- and $b\bar{b}$) than that of $\tau^+\tau^-$. The positron fraction and electron spectrum for the best fitting parameters are shown in Fig. 11. It is shown that the AMS-02 positron fraction data can be reproduced in this case.

However, it is well known that the PAMELA antiproton data and Fermi γ -ray data set very stringent constraints on the DM annihilation into quark and

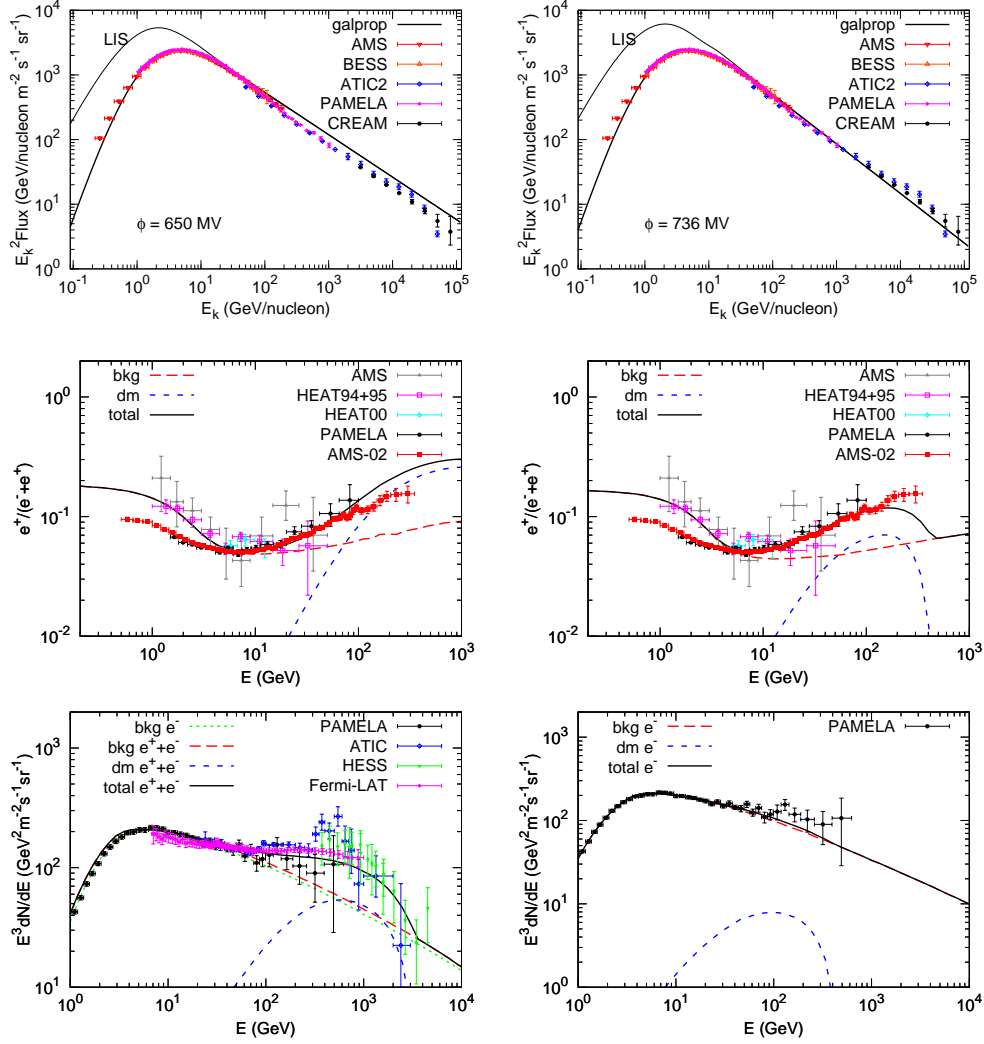


Figure 8: Same as Fig. 6 but the exotic e^\pm are assumed to be from DM annihilation. The annihilation channel is $\tau^+\tau^-$.

gauge boson final states[49, 50, 70, 71]. Fig. 12 shows the two dimensional contours on the $m_\chi - \langle\sigma v\rangle$ plane for the W^+W^- and $b\bar{b}$ channels and the 95% exclusion limits on DM annihilation to $b\bar{b}$ and W^+W^- channels by Fermi observation of dwarf galaxies [69]. It is shown that the DM scenario is disfavored to explain the e^\pm excesses.

Table 9: Fitting results of DM annihilation into $\tau^+\tau^-$ with proton spectrum relaxed

	I-b		II-b	
	best	mean	best	mean
$\log(A_p^1)$	-8.278	-8.282 ± 0.004	-8.310	-8.310 ± 0.005
ν_1	1.900	1.892 ± 0.023	1.962	1.951 ± 0.030
ν_2	2.281	2.285 ± 0.008	2.387	2.381 ± 0.012
$\log(p_{\text{br}}^p/\text{MeV})$	3.936	3.920 ± 0.032	4.136	4.101 ± 0.037
$\log(A_e^2)$	-8.962	-8.961 ± 0.004	-8.940	-8.944 ± 0.008
γ_1	1.512	1.534 ± 0.026	1.637	1.604 ± 0.056
γ_2	2.730	2.731 ± 0.011	2.794	2.792 ± 0.021
$\log(p_{\text{br}}^e/\text{MeV})$	3.558	3.569 ± 0.020	3.633	3.610 ± 0.027
$\log(m_\chi/\text{GeV})$	3.555	3.522 ± 0.075	2.657	2.670 ± 0.031
$\log(\langle\sigma v\rangle/\text{cm}^3\text{s}^{-1})$	-21.884	-21.929 ± 0.116	-23.222	-23.216 ± 0.048
c_{e^+}	1.856	1.875 ± 0.051	2.167	2.151 ± 0.094
ϕ/MV	650	649 ± 29	736	733 ± 47

¹Normalization at 100 GeV in unit of $\text{cm}^{-2}\text{s}^{-1}\text{sr}^{-1}\text{MeV}^{-1}$.

²Normalization at 25 GeV in unit of $\text{cm}^{-2}\text{s}^{-1}\text{sr}^{-1}\text{MeV}^{-1}$.

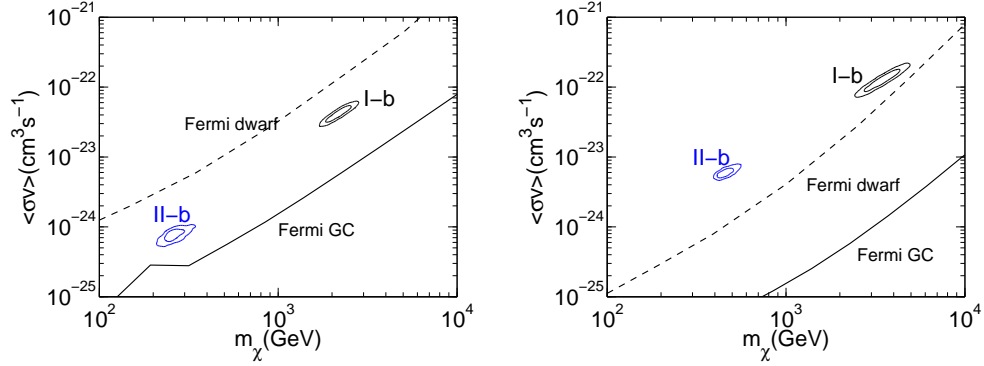


Figure 9: 1σ and 2σ confidence regions on the DM mass and cross section plane, for the fits I-b and II-b respectively. The left panel is for $\mu^+\mu^-$ channel, and the right panel is for $\tau^+\tau^-$ channel. The solid lines show the 95% upper limit of Fermi γ -ray observations of the Galactic center (with normalization of the local density corrected) [68] and dwarf galaxies [69].

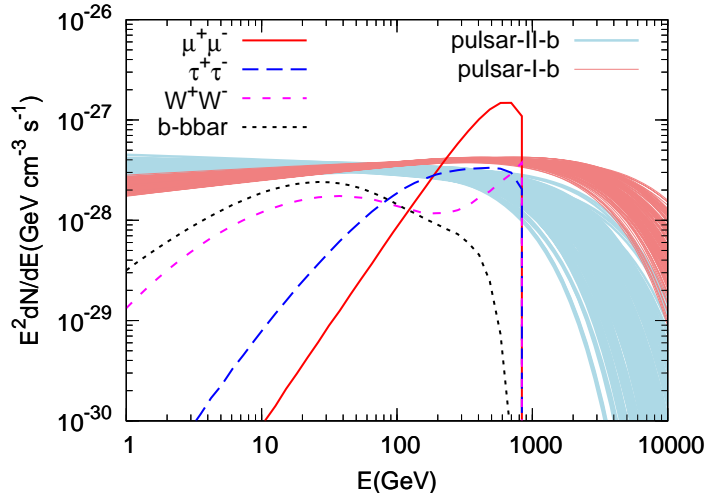


Figure 10: Shaded regions are 95% intervals of the exotic positron source component at the solar location of pulsar models. The DM-induced positron spectra for $\mu^+\mu^-$, $\tau^+\tau^-$, W^+W^- and $b\bar{b}$ channels are shown for comparison.

5. Discussion

5.1. Uncertainties of the theoretical model

Since the AMS-02 data are very precise, any uncertainties previously thought to be not important may affect the fitting result. As we note above the positron spectrum around tens of GeV may affect the fitting result sensitively. Therefore the change of the shape of background may affect the fitting results. There are quite a few sources of such uncertainties, such as the propagation parameters, the hadronic interaction models, and so on.

In this work we use the Kamae et al. (2006) parameterization of the pp collision [38]. As shown in [72] there were remarkable differences between different hadronic models. The Kamae et al. (2006) parameterization included more processes than before and was calibrated with recent data [38]. However, it depends strongly on the Monte Carlo simulations. Therefore we also test the fitting with old pp collision parameterization [73]. The results show quantitative difference from that shown above. But, all the conclusions made in the previous section keep unchanged.

We assume single power-law of the high energy (> 10 GeV) proton spectrum and neglect the spectral hardening around 200 GeV. Through introducing another break of the proton spectrum at ~ 230 GeV we can get better

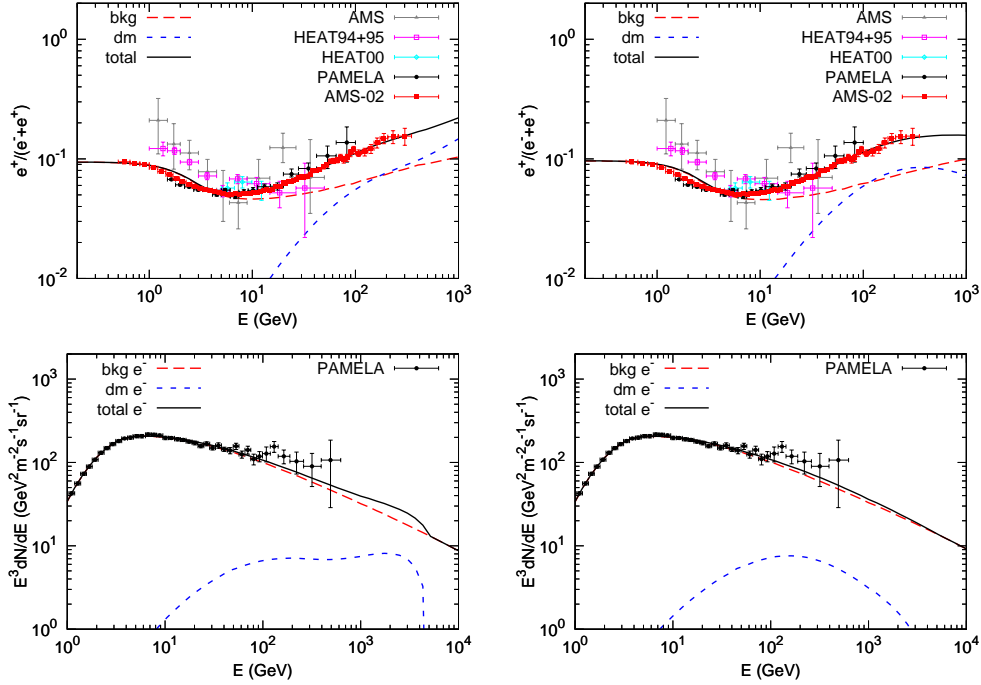


Figure 11: The positron fraction (top) and electron spectrum (bottom) for the best fitting parameters of the fit II-a with DM annihilation into W^+W^- (left) and $b\bar{b}$ (right) channels.

fit to the data. We have tested that in such a case the fitting results in this work change a little in numbers and the conclusions are not affected.

5.2. Alternatives of the primary electrons

As revealed by ATIC, CREAM and PAMELA measurements, the nuclei spectra have a hardening above ~ 200 GeV [57, 58, 19]. It is possible that the primary electron spectrum also has a similar hardening at high energies. By including such a modification of the primary electron spectrum may soften the *tension* and improve the fitting [74, 75].

It is also possible that the continuous assumption of the primary electron sources breaks down at energies above ~ 100 GeV. The variance due to nearby SNRs may result in deviation of the primary electron spectrum from power-law assumption and mimic the spectral hardening behavior [76]. In this case all the data may be fitted simultaneously.

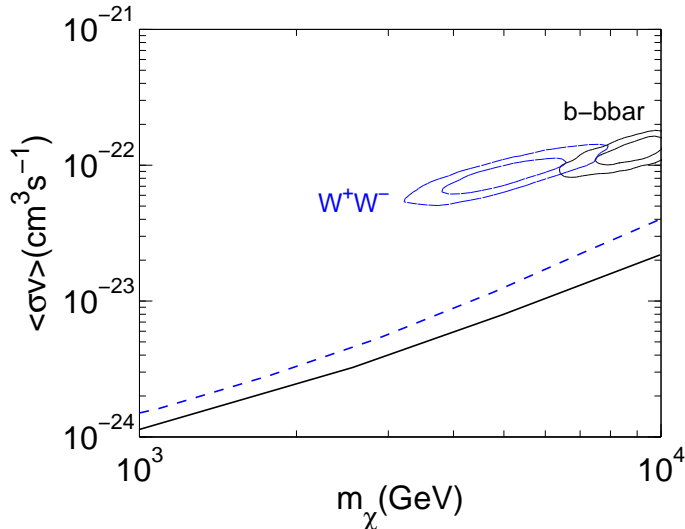


Figure 12: 1σ and 2σ confidence regions on the DM mass and cross section plane derived from fit II-a, for W^+W^- and $b\bar{b}$ channels. The lines show the upper limits derived using Fermi four year observations on the dwarf galaxies for W^+W^- (dashed) and $b\bar{b}$ (solid) channels [69].

5.3. Two or more components of the extra e^\pm sources

It is possible that there are more than one components of the primary sources of positrons. For example for the pulsar scenario, the far away pulsar population may contribute to a “background” component, and several nearby pulsars may give very distinct contributions to the positron spectrum [6]. Such a picture may help to improve the fitting to AMS-02 and Fermi/HESS e^\pm data. The “background” pulsars may give most contributions to the AMS-02 positron excesses, while the nearby sources can contribute mainly at high energies to reproduce the Fermi/HESS data. However, the detailed modeling in [77] seems that it is not easy to reconcile different datasets without changing the spectrum of the primary electrons.

5.4. To improve the DM scenario

Finally we discuss the possibilities to improve the DM scenario to give better explanation of the current data. First we need softer and broader spectrum of positrons from DM. Therefore if the annihilation final state is not two-body state but four-body, eight-body etc., softer positron spectrum may be generated. A mixture of leptonic channels and hadronic channels

may also give a broader spectrum (see Fig. 10). Second we have to consider how to avoid the constraints from γ -rays and antiprotons. Decaying DM scenario is better since the constraints from γ -rays are less stringent [78, 79]. As for the antiproton constraints, very massive DM particle may avoid the current bounds set by the PAMELA data [13].

6. Summary

In summary in this work we give a systematical investigation of the models to explain the cosmic e^\pm excesses, based on the newest AMS-02 data of the positron fraction and other data from PAMELA, Fermi and HESS. Both the pulsar-like scenario and DM scenario as the extra primary e^\pm sources are studied. Our findings are as follows.

- It is found that under the present framework it is difficult to fit the PAMELA/AMS-02 data and Fermi/HESS data simultaneously. The AMS-02 positron fraction data requires less positrons from the extra sources than that needed by Fermi/HESS data. It may indicate that either the model needs to be refined or there is inconsistency between different data sets. The latter possibility seems to be proved by the preliminary data of the total e^+e^- spectrum by AMS-02 [59].
- Pulsar-like models can fit the data better than the DM scenario. The spectral index of the positrons injected by the pulsars is about E^{-2} , which is much softer than that derived when using the PAMELA positron fraction data.
- If we fit only the AMS-02 positron fraction and PAMELA electron spectrum data both the pulsar-like and DM annihilates/decays into $\tau^+\tau^-$, W^+W^- and $b\bar{b}$ can fit the data. However, due to the lack of constraints from high energy range, these fits seem to under-estimate the contribution of the extra sources to the lepton fluxes.
- Due to the strong constraints from antiprotons and γ -rays, the DM annihilation scenario (into two body final states) seems not easy to be consistent with all of the current data.

Our study illustrates the remarkable potential on understanding the physics of the e^\pm excesses from the very precise measurement done by AMS-02. According to the PAMELA positron fraction data, the pulsar-like and DM

scenarios are almost identical [4]. Given the AMS-02 precise measurement, the differences between different scenarios become to appear. We are looking forward to more data with higher precision from AMS-02 to further shed light on the understanding of the fundamental questions of both astrophysics and particle physics.

Acknowledgments

We would like to thank Chen Hesheng, Hu Hongbo, Li Zuhao, Lü Yüsheng, Tang Zhicheng and Xu Weiwei for helpful discussions. This work is supported by 973 Program under Grant Nos. 2010CB83300 and 2013CB837000, and by National Natural Science Foundation of China under Grant Nos. 11075169, 11135009, 11105155 and 11220101004.

References

- [1] M. Aguilar, et al., Phys. Rev. Lett. **110**, 141102 (2013).
- [2] O. Adriani, et al., Nature **458**, 607 (2009), 0810.4995.
- [3] O. Adriani, et al., Astroparticle Physics **34**, 1 (2010), 1001.3522.
- [4] J. Liu, Q. Yuan, X.-J. Bi, H. Li, and X. Zhang, Phys. Rev. D **85**, 043507 (2012), 1106.3882.
- [5] H. Yüksel, M. D. Kistler, and T. Stanev, Phys. Rev. Lett. **103**, 051101 (2009), 0810.2784.
- [6] D. Hooper, P. Blasi, and P. Dario Serpico, J. Cosmol. Astropart. Phys. **1**, 25 (2009), 0810.1527.
- [7] S. Profumo, Central European Journal of Physics **10**, 1 (2012), 0812.4457.
- [8] D. Malyshev, I. Cholis, and J. Gelfand, Phys. Rev. D **80**, 063005 (2009), 0903.1310.
- [9] H.-B. Hu, Q. Yuan, B. Wang, C. Fan, J.-L. Zhang, and X.-J. Bi, Astrophys. J. Lett. **700**, L170 (2009), 0901.1520.
- [10] P. Blasi, Phys. Rev. Lett. **103**, 051104 (2009), 0903.2794.

- [11] L. Bergström, T. Bringmann, and J. Edsjö, Phys. Rev. D **78**, 103520 (2008), 0808.3725.
- [12] V. Barger, W.-Y. Keung, D. Marfatia, and G. Shaughnessy, Phys. Lett. B **672**, 141 (2009), 0809.0162.
- [13] M. Cirelli, M. Kadastik, M. Raidal, and A. Strumia, Nuclear Physics B **813**, 1 (2009), [Addendum-ibid. B **873**, 530 (2013)], 0809.2409.
- [14] P. F. Yin, Q. Yuan, J. Liu, J. Zhang, X. J. Bi, S. H. Zhu, and X. M. Zhang, Phys. Rev. D **79**, 023512 (2009), 0811.0176.
- [15] J. Zhang, X. J. Bi, J. Liu, S. M. Liu, P. F. Yin, Q. Yuan, and S. H. Zhu, Phys. Rev. D **80**, 023007 (2009), 0812.0522.
- [16] O. Adriani, et al., Phys. Rev. Lett. **106**, 201101 (2011).
- [17] O. Adriani, et al., Phys. Rev. Lett. **102**, 051101 (2009), 0810.4994.
- [18] O. Adriani, et al., Phys. Rev. Lett. **105**, 121101 (2010), 1007.0821.
- [19] O. Adriani, et al., Science **332**, 69 (2011), 1103.4055.
- [20] A. A. Abdo, et al., Phys. Rev. Lett. **102**, 181101 (2009), 0905.0025.
- [21] M. Ackermann, et al., Phys. Rev. D **82**, 092004 (2010).
- [22] J. Chang, et al., Nature **456**, 362 (2008).
- [23] F. Aharonian, et al., Phys. Rev. Lett. **101**, 261104 (2008), 0811.3894.
- [24] F. Aharonian, et al., Astron. Astrophys. **508**, 561 (2009), 0905.0105.
- [25] J. Liu, Q. Yuan, X. J. Bi, H. Li, and X. M. Zhang, Phys. Rev. D **81**, 023516 (2010), 0906.3858.
- [26] A. W. Strong and I. V. Moskalenko, Astrophys. J. **509**, 212 (1998), astro-ph/9807150.
- [27] T. K. Gaisser, *Cosmic rays and particle physics* (Cambridge and New York, Cambridge University Press, 1990, 292 p., 1990).
- [28] D. Maurin, F. Donato, R. Taillet, and P. Salati, Astrophys. J. **555**, 585 (2001).

- [29] G. di Bernardo, C. Evoli, D. Gaggero, D. Grasso, and L. Maccione, *Astroparticle Physics* **34**, 274 (2010), 0909.4548.
- [30] S. J. Lin, C. F. Cai, and et al., in preparation (2013).
- [31] A. W. Strong, I. V. Moskalenko, and V. S. Ptuskin, *Annual Review of Nuclear and Particle Science* **57**, 285 (2007), astro-ph/0701517.
- [32] E. S. Seo and V. S. Ptuskin, *Astrophys. J.* **431**, 705 (1994).
- [33] C. Evoli, D. Gaggero, D. Grasso, and L. Maccione, *J. Cosmol. Astropart. Phys.* **10**, 18 (2008), 0807.4730.
- [34] A. Putze, L. Derome, D. Maurin, L. Perotto, and R. Taillet, *Astron. Astrophys.* **497**, 991 (2009), 0808.2437.
- [35] A. Putze, L. Derome, and D. Maurin, *Astron. Astrophys.* **516**, A66 (2010), 1001.0551.
- [36] R. Trotta, G. Jóhannesson, I. V. Moskalenko, T. A. Porter, R. Ruiz de Austri, and A. W. Strong, *Astrophys. J.* **729**, 106 (2011), 1011.0037.
- [37] M. Ackermann, et al., *Astrophys. J.* **761**, 91 (2012), 1205.6474.
- [38] T. Kamae, N. Karlsson, T. Mizuno, T. Abe, and T. Koi, *Astrophys. J.* **647**, 692 (2006), astro-ph/0605581.
- [39] M. Mori, *Astroparticle Physics* **31**, 341 (2009), 0903.3260.
- [40] D. R. Lorimer, in *Young Neutron Stars and Their Environments*, edited by F. Camilo & B. M. Gaensler (2004), vol. 218 of *IAU Symposium*, p. 105.
- [41] Y. Fujita, K. Kohri, R. Yamazaki, and K. Ioka, *Phys. Rev. D* **80**, 063003 (2009), 0903.5298.
- [42] P. Blasi and P. D. Serpico, *Phys. Rev. Lett.* **103**, 081103 (2009), 0904.0871.
- [43] P. Mertsch and S. Sarkar, *Phys. Rev. Lett.* **103**, 081104 (2009), 0905.3152.

- [44] M. Ahlers, P. Mertsch, and S. Sarkar, *Phys. Rev. D* **80**, 123017 (2009), 0909.4060.
- [45] J. F. Navarro, C. S. Frenk, and S. D. M. White, *Astrophys. J.* **490**, 493 (1997), [astro-ph/9611107](#).
- [46] R. Catena and P. Ullio, *J. Cosmol. Astropart. Phys.* **8**, 4 (2010), 0907.0018.
- [47] P. Salucci, F. Nesti, G. Gentile, and C. Frigerio Martins, *Astron. Astrophys.* **523**, A83 (2010), 1003.3101.
- [48] M. Pato, O. Agertz, G. Bertone, B. Moore, and R. Teyssier, *Phys. Rev. D* **82**, 023531 (2010), 1006.1322.
- [49] F. Donato, D. Maurin, P. Brun, T. Delahaye, and P. Salati, *Phys. Rev. Lett.* **102**, 071301 (2009), 0810.5292.
- [50] I. Cholis, *J. Cosmol. Astropart. Phys.* **9**, 007 (2011), 1007.1160.
- [51] T. Sjöstrand, S. Mrenna, and P. Skands, *Journal of High Energy Physics* **5**, 26 (2006), [hep-ph/0603175](#).
- [52] L. J. Gleeson and W. I. Axford, *Astrophys. J.* **154**, 1011 (1968).
- [53] J. M. Clem, D. P. Clements, J. Esposito, P. Evenson, D. Huber, J. L'Heureux, P. Meyer, and C. Constantin, *Astrophys. J.* **464**, 507 (1996).
- [54] B. Beischer, P. von Doetinchem, H. Gast, T. Kirn, and S. Schael, *New Journal of Physics* **11**, 105021 (2009).
- [55] S. Della Torre, et al., *Advances in Space Research* **49**, 1587 (2012).
- [56] L. Maccione, *Phys. Rev. Lett.* **110**, 081101 (2013), 1211.6905.
- [57] A. D. Panov, et al., *Bulletin of the Russian Academy of Science, Phys.* **71**, 494 (2007), [astro-ph/0612377](#).
- [58] H. S. Ahn, et al., *Astrophys. J. Lett.* **714**, L89 (2010), 1004.1123.

- [59] AMS-02 collaboration, in *International Cosmic Ray Conference* (<http://www.ams02.org/2013/07/new-results-from-ams-presented-at-icrc-2013/>, 2013).
- [60] Q. Yuan, B. Zhang, and X.-J. Bi, *Phys. Rev. D* **84**, 043002 (2011), 1104.3357.
- [61] J. Alcaraz, et al., *Phys. Lett. B* **490**, 27 (2000).
- [62] T. Sanuki, et al., *Astrophys. J.* **545**, 1135 (2000), [astro-ph/0002481](#).
- [63] M. Aguilar, et al., *Phys. Lett. B* **646**, 145 (2007), [astro-ph/0703154](#).
- [64] S. W. Barwick, et al., *Astrophys. J. Lett.* **482**, L191 (1997), [astro-ph/9703192](#).
- [65] S. Coutu, et al., in *International Cosmic Ray Conference* (2001), vol. 5 of *International Cosmic Ray Conference*, p. 1687.
- [66] H.-B. Jin, Y.-L. Wu, and Y.-F. Zhou, *J. Cosmol. Astropart. Phys.* **11**, 026 (2013), 1304.1997.
- [67] I. Cholis and D. Hooper, *Phys. Rev. D* **88**, 023013 (2013), 1304.1840.
- [68] X. Huang, Q. Yuan, P.-F. Yin, X.-J. Bi, and X. Chen, *J. Cosmol. Astropart. Phys.* **11**, 048 (2012), 1208.0267.
- [69] A. Drlica-Wagner, in *Fermi Symposium 2012* (2012).
- [70] M. Ackermann, et al., *Phys. Rev. Lett.* **107**, 241302 (2011), 1108.3546.
- [71] A. Geringer-Sameth and S. M. Koushiappas, *Phys. Rev. Lett.* **107**, 241303 (2011), 1108.2914.
- [72] T. Delahaye, R. Lineros, F. Donato, N. Fornengo, J. Lavalle, P. Salati, and R. Taillet, *Astron. Astrophys.* **501**, 821 (2009), 0809.5268.
- [73] G. D. Badhwar, R. L. Golden, and S. A. Stephens, *Phys. Rev. D* **15**, 820 (1977).
- [74] L. Feng, R.-Z. Yang, H.-N. He, T.-K. Dong, Y.-Z. Fan, and J. Chang, *Physics Letters B* **728**, 250 (2014), 1303.0530.

- [75] Q. Yuan and X.-J. Bi, Physics Letters B **727**, 1 (2013), 1304.2687.
- [76] M. Di Mauro, F. Donato, N. Fornengo, R. Lineros, and A. Vittino, J. Cosmol. Astropart. Phys. **04**, 006 (2014), 1402.0321.
- [77] P.-F. Yin, Z.-H. Yu, Q. Yuan, and X.-J. Bi, Phys. Rev. D **88**, 023001 (2013), 1304.4128.
- [78] M. Papucci and A. Strumia, J. Cosmol. Astropart. Phys. **3**, 14 (2010), 0912.0742.
- [79] M. Cirelli, P. Panci, and P. D. Serpico, Nuclear Physics B **840**, 284 (2010), 0912.0663.